Research Square

Preprints are preliminary reports that have not undergone peer review.
They should not be considered conclusive, used to inform clinical practice,
or referenced by the media as validated information.

Astragalus polysaccharide ameliorates adipogenic skewing and dysfunction of bone marrow mesenchymal stromal cells in aplastic anemia via mTOR inhibition

Xiaoyan Hou

hxy8803@yeah.net

Longdong University

Xiaoling Zhou

Xifeng District People's Hospital

Jie Wang

Qingyang Hospital of Traditional Chinese Medicine

Jing Huang

Longdong University

Boping Li

Longdong University

Liya Feng

Longdong University

Jinlong Kai

Qingyang Rehabilitation Hospital

Article

Keywords: Aplastic anemia, Bone marrow mesenchymal stem cells, Astragalus polysaccharides, Adipogenic differentiation, mTOR

Posted Date: August 20th, 2026

DOI: https://doi.org/10.21203/rs.3.rs-10457318/v1

License: This work is licensed under a Creative Commons Attribution 4.0 International License.
Read Full License

Additional Declarations: No competing interests reported.

Abstract

BM-MSCs from aplastic anemia (AA) patients show impaired proliferation, elevated apoptosis, and aberrant adipogenic differentiation, thereby generating a microenvironment that inhibits hematopoiesis. Astragalus polysaccharide (APS), a regenerative bioactive component extracted from Astragalus membranaceus, has unclear effects on AA-BM-MSCs. In this study, AA-BM-MSCs were exposed to APS (0–4000 μg/mL). Based on dose–response analysis, control, low-dose (62.5 μg/mL), and high-dose (1000 μg/mL) groups were selected for 48 h treatment. Proliferation, apoptosis, cell cycle, and lipid accumulation were assessed by CCK-8, flow cytometry, and Nile Red staining, respectively, while the mRNA and protein levels of adipogenic markers (PPARγ, CFD, LPL) and mTOR pathway components were quantified via RT-qPCR and Western blot. Results showed that APS dose-dependently enhanced proliferation and suppressed apoptosis. High-dose APS promoted S/G2/M phase progression. APS also reduced lipid droplets and downregulated PPARγ, CFD, and LPL, and currently attenuated mTOR hyperactivation. In conclusion, APS ameliorates BM-MSC dysfunction in AA by restoring proliferation, inhibiting apoptosis, and suppressing aberrant adipogenesis, likely through mTOR pathway inhibition, thereby repairing the stromal niche to support hematopoiesis.

1. Introduction

Aplastic anemia (AA) is an uncommon but severe bone marrow failure syndrome, which is clinically characterized by peripheral blood pancytopenia and hypocellular bone marrow with deficiency of hematopoietic precursors, and no evidence of cell infiltration or fibrosis can be detected in the affected bone marrow [1, 2]. The core pathogenic mechanism of acquired AA is widely accepted to be immune-mediated destruction of HSPCs driven by autoreactive T lymphocytes [3, 4]. Nevertheless, growing evidence indicates that bone marrow microenvironmental dysfunction, especially that involving bone marrow mesenchymal stem/stromal cells (BM-MSCs), exerts a non-negligible effect on the onset and progression of this disease, which has long been underappreciated [5, 6].

BM-MSCs are multipotent stromal cells critical to hematopoietic niche homeostasis. They maintain this balance through direct cell–cell contacts, paracrine release of cytokines and growth factors, and tightly controlled differentiation into osteoblasts, chondrocytes, and adipocytes [7]. Under physiological conditions, osteolineage cells facilitate hematopoiesis, whereas excessive adipogenesis generates an inhibitory microenvironment that impairs HSPC function [8, 9]. BM-MSCs derived from AA patients present persistent functional defects: weakened proliferation, elevated senescence and apoptosis, G0/G1 cell cycle arrest, and a differentiation shift toward adipogenesis with suppressed osteogenic potential [10]. This pathological “fatty marrow“ phenotype loses hematopoietic supportive capacity and further triggers HSPC depletion through abnormal secretory profiles and metabolic disturbances [11].

The molecular mechanisms underlying aberrant MSC function in AA have not been fully elucidated. Nevertheless, accumulating evidence indicates dysregulation of the phosphatidylinositol 3-kinase (PI3K)–Akt–mammalian target of rapamycin (mTOR) signaling axis. This pathway integrates multiple

extracellular signals to regulate cell survival, proliferation, metabolism and cell lineage differentiation [12]. Moderate transient mTOR activation facilitates MSC proliferation, while persistent mTORC1 overactivation accelerates adipogenic differentiation via upregulating master transcription factors including PPARγ and C/EBPα [13, 14]. Elevated phosphorylation levels of Akt and mTOR are observed in BM-MSCs isolated from AA patients, which is correlated with excessive lipid deposition and weakened hematopoietic supporting capacity. Rapamycin-mediated pharmacological inhibition of mTOR recovers osteogenic capacity and blocks abnormal adipogenesis in damaged MSCs [15], indicating this signaling axis is a promising therapeutic target.

Astragalus membranaceus (Huang Qi), a traditional Chinese herb long used for “tonifying Qi” and restoring vitality, has served as an adjunct to immunosuppressive therapy in aplastic anemia (AA) for decades [16]. Its major bioactive component, Astragalus polysaccharide (APS), exhibits diverse pharmacological properties, including immunomodulation, antioxidation, anti-apoptotic effects, and promotion of tissue regeneration [17]. A growing body of preclinical evidence has revealed that APS and other Astragalus-derived compounds modulate key signaling pathways in a context-dependent manner to mitigate pathological damage across multiple disease models. For instance, APS improves vascular endothelial dysfunction by driving macrophage M2 polarization via activation of the Nrf2/HO-1 pathway, underscoring its potential to resolve inflammation and restore tissue homeostasis [18]. APS exerts complex, bidirectional regulation on the Nrf2/HO-1 axis. In murine experimental colitis and human Caco-2 cells, APS inhibits ferroptosis through modulation of this pathway, highlighting its ability to fine-tune signaling cascades according to the prevailing pathological microenvironment. Beyond polysaccharides, astragalus polyphenols (APP) also confer significant cytoprotection. APP attenuates doxorubicin-induced cardiotoxicity by activating the PI3K/AKT/NRF2 pathway, enhancing antioxidant defenses and suppressing apoptotic signaling in cardiomyocytes [19]. Moreover, APS alleviates bleomycin-induced pulmonary fibrosis by suppressing the pro-inflammatory TLR4/NF-κB pathway to reduce excessive cytokine production, while concurrently modulating gut microbiota composition—potentially exerting indirect anti-fibrotic effects through the gut–lung axis [20].

However, it remains unclear whether APS is capable of reversing intrinsic functional defects in AA-BM-MSCs, especially their pathological tendency toward adipogenic differentiation, and whether the PI3K-Akt-mTOR signaling axis mediates these protective effects. Given that MSC dysfunction occupies a core position in AA pathogenesis and sustained mTOR overactivation is tightly associated with biased adipogenic differentiation, we proposed the hypothesis that APS exerts protective effects on AA-BM-MSCs via inhibiting abnormal mTOR signaling, thus restoring cell proliferative ability and balancing cell differentiation fate.

In this study, BM-MSCs were isolated from treatment-naïve AA patients. We systematically evaluated the influences of APS on cell proliferation, apoptosis, cell cycle distribution and adipogenic differentiation. The expression and phosphorylation levels of core molecules within the PI3K-Akt-mTOR pathway as well as downstream adipogenic transcription factors were further detected. Our findings reveal the underlying

mechanism by which APS improves AA through targeting bone marrow mesenchymal stem cell niche, indicating APS may serve as a promising therapeutic candidate for AA treatment.

2. Materials and Methods

2.1 Patients and Ethical Approval

Bone marrow samples were prospectively collected from 21 patients with newly diagnosed, treatment-naïve acquired aplastic anemia (AA) who presented to the Department of Hematology, Qingyang Hospital of Traditional Chinese Medicine between April 2022 and April 2025. The 21 patients (16 women and 5 men) had a median age of 52 years (range, 16–72). AA was diagnosed according to established clinical criteria incorporating peripheral blood examination, bone marrow aspiration, and biopsy. Written informed consent was provided by all participants before sample collection. The study was approved by the Institutional Ethics Committee of Qingyang Hospital of Traditional Chinese Medicine (Approval No. QYTCM20210011) and conducted in accordance with the Declaration of Helsinki.

2.2 Isolation and Culture of BM-MSCs

Bone marrow mononuclear cells (BM-MNCs) were separated via Ficoll-Paque PLUS (GE Healthcare) density gradient centrifugation. The interfacial mononuclear cell layer was harvested, rinsed twice with PBS, and resuspended in complete culture medium. The medium was prepared with DMEM/F-12 (Gibco, 21041025) supplemented with 10% fetal bovine serum (ExCell Bio, 111323), 1% penicillin-streptomycin solution (Procell, PB180225), 10 ng/mL EGF (PeproTech, AF-100-15-100) and 10 ng/mL bFGF (PeproTech, 100-18B-100). Isolated cells were seeded in T25 culture flasks at a density of 1×10^6 cells/cm² and incubated at 37°C with 5% humidified CO_2.Culture medium was refreshed every 3–4 days to eliminate non-adherent cells, and routine mycoplasma monitoring was performed to ensure sterile culture conditions. When adherent spindle-shaped cells reached 80–90% confluence, 0.25% trypsin-EDTA (Procell, PB180225) was used for cell digestion and subculture, and cells at appropriate passages were used for subsequent experiments

2.3 Network Pharmacology Analysis

The chemical constituents of Astragalus membranaceus were retrieved from the Traditional Chinese Medicine Systems Pharmacology Database (TCMSP) and screened by oral bioavailability (OB) ≥ 30% and drug-likeness (DL) ≥ 0.20. The candidate compounds were further validated by the SwissADME platform, and high-confidence active ingredients with good gastrointestinal absorption and favourable drug-likeness were retained. Their putative protein targets were predicted using SwissTargetPrediction (probability ≥ 0.1, Homo sapiens), yielding unique human targets after deduplication and UniProt standardisation. Aplastic anaemia-related genes were retrieved from the GeneCards database (relevance score > median). The intersection between compound targets and disease genes was determined using Venny 2.1.0. A protein–protein interaction (PPI) network was constructed in STRING (confidence ≥

0.400) and analysed in Cytoscape 3.9.1 with the CytoHubba plugin (Degree algorithm) to identify hub nodes. Gene Ontology (GO) and Kyoto Encyclopedia of Genes and Genomes (KEGG) enrichment analyses of the shared targets were performed using Metascape (FDR < 0.05, Benjamini–Hochberg correction), and visualised with SRplot and ggplot2 in R.

.2.4 Characterization of BM-MSCs

Prior to experiments, the isolated cells were authenticated by flow cytometry (CytoFLEX, Beckman Coulter). The cells were stained with fluorochrome-conjugated antibodies against positive markers (CD29, CD44, CD105, CD106, CD309) and negative markers (CD31, CD11a, CD11b, CD34, HLA-DR), all from BioLegend (Cat. Nos. 303003, 338807, 305805, 359903, 800503, 303105, 301207, 301305, 343605, 327007). The cells displayed high expression of the positive markers and lacked CD34, conforming to a surface profile typical of MSCs. Only populations exceeding 95% purity were used for subsequent experiments.

2.5 APS Preparation and Treatment

APS (purity ≥ 50%) was obtained from Solarbio (Beijing, China; Cat. No. A7970) and its identity and purity were verified by the manufacturer via HPLC. A 40 mg/mL stock solution was prepared in sterile PBS, filtered (0.22 μm), and stored at − 20°C. For dose–response assays, BM-MSCs were exposed to APS at 0–4000 μg/mL for 48 h.

2.6 Cell Proliferation Assay

Cell proliferative ability was assessed using the CCK-8 kit (Biotopped, LF696-500T). Cells in the logarithmic growth phase were inoculated into 96-well plates at a density of 2×10^4 cells per well, with a final volume of 100 μL medium per well and three replicate wells set for each condition. After complete cell attachment, APS working solution was supplemented to generate gradient final concentrations ranging from 0 μg/mL to 4000 μg/mL (0, 62.5, 125, 250, 500, 1000, 2000, and 4000 μg/mL). At 24, 36, 48, and 72 h after treatment, 10 μL of CCK-8 reagent was dispensed into each well. Following 1 h of incubation, the optical density value at 450 nm was detected for cell viability analysis.

2.7 Apoptosis Analysis

Apoptosis was analyzed using an Annexin V-FITC/PI detection kit (KeyGEN BioTECH, Cat. No. KGA108). After 48 h of APS treatment, cells were collected, dual-stained with Annexin V-FITC and PI, and analyzed within 1 h by flow cytometry (CytoFLEX, Beckman Coulter).

2.8 Cell Cycle Analysis

Cells were fixed in 70% ice-cold ethanol and maintained overnight at -20°C. They were then stained with propidium iodide (Beyotime, Catalogue No. ST511) in the presence of RNase A for 30 minutes at 37°C in a dark environment. DNA content was subsequently analyzed via flow cytometry (CytoFLEX), and cell cycle distribution was determined using FlowJo software.

2.9 Adipogenic Differentiation Assay

BM-MSCs were pre-treated with APS for a duration of 48 hours. Subsequently, the cells were induced to undergo adipogenic differentiation over a 21-day period using an Iscove's Modified Dulbecco's Medium (IMDM)-based adipogenic induction medium (Immocell, Catalogue No. IMC-203). This medium was supplemented with dexamethasone, 3-isobutyl-1-methylxanthine (IBMX), insulin, and indomethacin, while APS was continuously maintained throughout the induction phase. On the 21st day, intracellular lipid droplets were stained with Nile red (Sourceleaf Bio, Catalogue No. S19279; concentration: 1 μg/mL in PBS, incubation: 10 minutes at room temperature) and subsequently visualized using either an inverted fluorescence microscope (Mshot) or a confocal laser scanning microscope (Nikon Eclipse Ti equipped with Eclipse C2 imaging software). For quantitative analysis, the fluorescence of Nile red was extracted using isopropanol and measured at excitation/emission wavelengths of 485/535 nm with a BioTek microplate reader.

2.10 Quantitative Real-Time PCR (RT-qPCR)

Total RNA was isolated employing the TRIzol reagent (Invitrogen, Catalogue No. 15596026), followed by the synthesis of complementary DNA (cDNA) utilizing a reverse transcription kit (Vazyme, Catalogue No. R223-01). RT-qPCR was conducted on a QuantStudio 6 Real-Time PCR System (Applied Biosystems) with the application of SYBR Green Master Mix (Vazyme, Catalogue No. Q111-02). Specific primers targeting *PPARγ*, *CFD*, *LPL*, and *GAPDH* (internal control) were employed, as detailed in Supplementary Table S1. The relative expression levels of the genes were determined using the $2^{-\Delta\Delta Ct}$ method.

2.11 Western Blot Analysis

Cells were lysed using RIPA buffer supplemented with protease and phosphatase inhibitors. Proteins (30 μg per sample) were resolved via SDS-PAGE and subsequently transferred onto PVDF membranes. The membranes were treated with 5% non-fat milk to block them and then incubated overnight at 4°C with primary antibodies targeting CFD (Abclonal, Catalogue No. A21110), LPL (Affinity, Catalogue No. BF0636), PPARγ (Affinity,Catalogue No. AF6284), 4EBP1 (Affinity, Catalogue No. AF6432), P70S6K (Affinity, Catalogue No. AF6226), mTOR and phospho-mTOR (Ser2448) (Proteintech, Catalogue No. 67778-1-Ig), and β-actin (Affinity, Catalogue No. T0022). Following incubation with horseradish peroxidase (HRP)-conjugated secondary antibodies, signals were detected utilizing an enhanced chemiluminescence substrate and subsequently visualized with a chemiluminescence imaging system. ImageJ software (NIH) was used to quantify the band intensities.

2.12 Statistical Analysis

Data are presented as mean ± standard deviation (SD). For in vitro assays, each experiment was performed using BM-MSCs derived from at least three independent patients, with technical triplicates for each patient. Normality was assessed using the Shapiro-Wilk test, and homogeneity of variance was confirmed by Levene's test prior to one-way ANOVA. Post hoc comparisons were performed using Tukey's test. A two-tailed P-value < 0.05 was considered statistically significant.

3. Results

3.1 Network pharmacology identifies core targets and pathways linking Astragalus to AA-related MSC imbalance

To study the molecular mechanisms of the therapeutic effects of APS in the treatment of AA, network pharmacology was used, and bioactive small-molecule components of Astragalus membranaceus were taken as proxies for systemic activity. First, 20 bioactive compounds were obtained from the Traditional Chinese Medicine Systems Pharmacology Database (TCMSP) based on the screening criteria of oral bioavailability (OB) ≥ 30% and drug-likeness (DL) ≥ 0.20 (Supplementary Table S2). To increase the accuracy of compound selection, the above candidates were further validated by the SwissADME platform, and only those with good gastrointestinal (GI) absorption and at least two positive indicators in the drug-likeness assessment were retained. Through the above optimisation steps, 13 high-confidence active ingredients were identified, which include well-known isoflavonoids such as calycosin, formononetin, quercetin and kaempferol, as well as some pterocarpan derivatives (e.g., 9,10-dimethoxypterocarpan-3-O-β-D-glucoside).

Based on the predictions from SwissTargetPrediction for the 13 putative protein targets of these compounds, a total of 902 unique human targets were obtained. At the same time, 3,395 genes related to aplastic anaemia were obtained from the GeneCards database. The intersection of the two sets of data identified 149 overlapping targets and proposed that Astragalus might influence the disease process of AA and MSC differentiation at a molecular level (Fig. 1A).

Functional enrichment analysis of the 149 shared targets showed that they participated in several biological processes and signaling pathways significantly. Gene Ontology (GO) enrichment analysis indicated that these 149 targets were mainly located in membrane rafts and protein kinase complexes (Cellular Component, Fig. 1B), were enriched in transmembrane receptor tyrosine kinase and serine/threonine kinase activities (Molecular Function, Fig. 1C), and participated in peptidyl-serine phosphorylation and protein kinase B (Akt) signaling (Biological Process, Fig. 1D). Collectively, the above results show that Astragalus membranaceus regulates the activity of membrane-associated receptor-mediated signaling pathways by altering kinase activation and phosphorylation.

KEGG pathway analysis further shows that several PI3K-Akt, mTOR, FoxO, MAPK and apoptosis pathways are significantly enriched (Fig. 1E). The PI3K-Akt-mTOR pathway was relatively more abundant in the KEGG enrichment analysis. Analysis of the protein-protein interaction (PPI) network identified AKT1, EGFR, JUN, MAPK1, and MTOR as hub nodes, and these may be responsible for the biological effects of Astragalus membranaceus (Fig. 1F). As a high-value bioactive substance of this herb, APS is believed to be responsible for regulating the signalling pathway mentioned above and consequently affecting the differentiation of MSCs.

3.2 Astragalus membranaceus Inhibit the PI3K-Akt-mTOR Signaling Pathway in Aplastic Anemia-Derived BM-MSCs

To experimentally verify the hypothesis that Astragalus membranaceus inhibits the overactive PI3K-AKT-mTOR signaling axis in AA, we isolated bone marrow mesenchymal stem cells (BM-MSCs) from AA patients and treated them with either purified APS or crude aqueous extract (AQE).

Flow cytometry confirmed that the isolated MSCs were uniform and highly expressed the mesenchymal markers CD29 (97.78%), CD44 (98.07%), CD105 (98.36%), CD106 (98.15%), and CD309 (98.43%), with little to no expression of the hematopoietic marker CD34 (0.09%) (Fig. 2A).

Subsequent Western blot analysis showed that both APS and AQE effectively inhibited the phosphorylation of key signaling nodes AKT and mTOR in a concentration-dependent manner (Fig. 2B and C). 62.5 μg/mL APS or AQE treatment did not significantly change the phosphorylation levels of AKT or mTOR, and the signal intensity was comparable to that of the untreated control. On the other hand, exposure to 1000 μg/mL of either APS or AQE resulted in a significant reduction of both p-Akt and p-mTOR, thus inhibiting the PI3K-AKT-mTOR pathway effectively at high concentrations. The total amounts of Akt and mTOR proteins were the same under all treatment conditions; thus, the change observed was due to altered pathway activation rather than a reduction in total protein levels.

Together, these results provide direct experimental evidence that both the purified APS and the whole AQE of Astragalus membranaceus can downregulate the abnormally active PI3K-AKT-mTOR pathway in AA-derived BM-MSCs, and thus support their potential for restoring MSC homeostasis and hematopoietic support function in aplastic anemia.

3.3 Astragalus Polysaccharide Enhances Proliferation, Suppresses Apoptosis, and Modulates Cell Cycle in AA-Derived BM-MSCs

APS is widely regarded as a principal bioactive fraction of AQE. We elected to use purified APS to clearly delineate the functional effects attributable to this key polysaccharide component.

Initial CCK-8 assays revealed that APS enhanced the viability of BM-MSCs from patients with AA in a time- and concentration-dependent manner, with maximal proliferative stimulation observed at 48 h ($P < 0.05$, Fig. 3A). Importantly, no cytotoxicity was detected even at concentrations up to 4000 μg/mL, indicating a wide therapeutic window for APS in human MSCs. Based on this dose–response profile, we selected 62.5 μg/mL (a concentration yielding minimal proliferative effect) and 1000 μg/mL (the dose producing peak viability) for subsequent functional assays to capture responses across the activity spectrum.

At both concentrations, APS significantly suppressed apoptosis in AA-BM-MSCs. The total apoptotic fraction decreased from 8.06% ± 0.42% in untreated controls to 5.90% ± 0.25% with 62.5 μg/mL APS ($P < 0.001$) and further to 2.07% ± 0.21% with 1000 μg/mL APS ($P < 0.001$), with a significant difference between the two treatment groups ($P < 0.001$; Fig. 3B and C).

Concomitantly, APS induced a profound shift in cell cycle distribution (Fig. 3D and E). Compared to control cells (G0/G1: 53.16% ± 0.28%), treatment with 62.5 μg/mL APS reduced G0/G1 occupancy to 33.59% ± 0.60% ($P < 0.05$) and increased S phase and G2/M phase. These effects were markedly amplified at 1000 μg/mL APS, where only 21.03% ± 2.02% of cells remained in G0/G1, while S and G2/M populations rose to 40.41% ± 0.84% and 38.56% ± 1.49%, respectively ($P < 0.05$). This concentration-dependent progression through the cell cycle aligns with the observed proliferative and anti-apoptotic effects.

Collectively, the above data show that purified APS can restore several functions of AA-derived BM-MSCs: it promotes proliferation, suppresses apoptosis, induces cell cycle progression, and inhibits abnormal adipogenic differentiation. The consistent dose-dependent effect of all assays indicates that it is biologically active and can be used to target MSC dysfunction in aplastic anaemia for therapy.

3.4 APS Inhibits Adipogenic Gene Expression and mTORC1 Signaling in AA-Derived BM-MSCs

To define the mechanism underlying APS-mediated inhibition of adipogenesis, we examined adipogenic markers and mTOR pathway components at both mRNA and protein levels (Fig. 4).

Confocal imaging revealed a dose-dependent reduction in intracellular lipid droplets: abundant red fluorescence in control cells was markedly diminished at 62.5 μg/mL APS and nearly absent at 1000 μg/mL, confirming potent, concentration-dependent suppression of lipid accumulation (Fig. 4A).

RT-qPCR analysis showed that mRNA levels of the adipogenic regulators CFD, LPL, and PPARγ were significantly lower in both APS-treated groups relative to control ($P < 0.05$). In parallel, transcript levels of the mTORC1 downstream effectors 4E-BP1 and p70S6K decreased in a concentration-dependent manner (Fig. 4B).

These changes were paralleled at the protein level. Western blotting demonstrated a dose-dependent decline in CFD, LPL, PPARγ, 4E-BP1, and p70S6K protein expression (Fig. 4C). Notably, total mTOR abundance remained unchanged, whereas phosphorylated mTOR (p-mTOR) was significantly reduced by APS, especially at 1000 μg/mL, indicating that APS suppresses mTOR kinase activity without affecting total protein levels.

Collectively, these data indicate that APS counteracts adipogenic commitment in AA-derived BM-MSCs by downregulating PPARγ,CFD,andLPLand by attenuating mTORC1 signaling through decreased mTOR phosphorylation.

4. Discussion

Aplastic anemia is classically defined as an immune-driven bone marrow failure disorder primarily caused by the immune destruction of hematopoietic stem and progenitor cells (HSPCs). Nevertheless, growing clinical and basic research confirms that abnormalities in the bone marrow microenvironment, especially functional defects of BM-MSCs, are indispensable contributors to AA pathogenesis [24]. In AA patients, endogenous BM-MSCs commonly present inferior proliferative activity, excessive apoptosis, G0/G1 phase cell cycle arrest, and a distinct differentiation shift toward adipogenesis with compromised osteogenic differentiation [5, 6]. The resulting fatty marrow phenotype loses normal hematopoietic supportive function. Abnormal cytokine secretion and metabolic disorders further impair HSPC activity, ultimately aggravating bone marrow hematopoietic failure [25]. Accordingly, recovering the biological function of BM-MSCs is considered a viable therapeutic strategy for AA intervention.

The present study validated the protective effects of APS on dysfunctional AA-BM-MSCs. CCK-8 results demonstrated that APS improved the viability of AA-BM-MSCs in a concentration-dependent manner. Flow cytometry analysis further verified that APS intervention alleviated cell apoptosis and facilitated cell cycle transition from the G0/G1 phase to S/G2 phases. Collectively, these results suggest that APS can effectively restore the proliferative ability and biological activity of damaged BM-MSCs, which helps rebuild a functional bone marrow hematopoietic microenvironment.

This study confirmed the regulatory effect of APS on the abnormal adipogenic differentiation of AA-BM-MSCs. Nile Red staining showed that APS intervention markedly reduced intracellular lipid deposition in pathological MSCs. Consistent with the phenotypic improvement, molecular detection results also supported the reversal of abnormal adipogenesis: APS significantly downregulated the mRNA and protein levels of the core adipogenic transcription factor PPARγ, as well as its downstream functional genes CFD and LPL. Since PPARγ is the central regulator governing MSC adipogenic programming, the downregulation of PPARγ is the key molecular basis for APS to inhibit excessive adipogenesis. Consistent with previous reports on the adipogenic differentiation bias of AA-BM-MSCs, our study innovatively verified that APS could reverse this pathological differentiation tendency.

To further explore the potential molecular mechanism of APS, this study focused on the PI3K-AKT-mTOR signaling axis, which was previously identified as the core therapeutic target of Astragalus for AA treatment. Existing studies have confirmed that sustained activation of mTORC1 signaling promotes MSC adipogenic differentiation by upregulating PPARγ and C/EBPα. In line with clinical findings [26], our experiment also detected elevated phosphorylation levels of Akt and mTOR in AA-BM-MSCs, indicating abnormal overactivation of the mTOR pathway in pathological MSCs. Notably, high-dose APS intervention obviously inhibited the phosphorylation of mTOR without affecting total mTOR protein expression. Meanwhile, the levels of classic mTORC1 downstream effector molecules p70S6K and 4E-BP1 were also significantly decreased. These findings indicate that APS suppresses the abnormal activation of the mTOR signaling pathway by reducing mTOR phosphorylation, thereby inhibiting the excessive adipogenic differentiation of AA-BM-MSCs.

5. Conclusion

In conclusion, this study clarifies the regulatory mechanism by which APS improves AA-BM-MSC dysfunction via inhibiting the overactivated PI3K-AKT-mTOR pathway. APS exerts dual protective effects on AA-BM-MSCs: it enhances cell proliferation and survival, while restraining pathological adipogenic differentiation, thereby restoring bone marrow microenvironment homeostasis. This study provides experimental evidence and molecular basis for the clinical adjuvant application of Astragalus in AA treatment. Meanwhile, it confirms the potential of targeting BM-MSC signaling abnormalities for AA therapy. Subsequent in vivo animal experiments are required to further verify the above therapeutic effects of APS. In addition, the effects of APS on MSC immunoregulation, osteogenic differentiation and hematopoietic supporting function need to be further explored to comprehensively evaluate its clinical transformation value.

Declarations

Funding

This work was supported by the Natural Science Foundation of Gansu Province (No. 25JRRM002) and the Innovation Fund Project of the Education Department of Gansu Province (No. 2023B-212 and 2026A-206).

Author contributions

Xiaoyan Hou: Conceptualization, Data curation, Data curation, Funding acquisition, Writing-Original Draft. Xiaoling Zhou: Data curation, Validation, Writing-Original Draft. Jie Wang: Data curation. Jing Huang: Formal analysis, Funding acquisition, Writing-Original Draft. Boping Li: Formal analysis, Funding acquisition,Writing-Original Draft. Liya Feng : Writing-review & editing. Jinlong Kai: Supervision, Writing-Review & Editing.

Ethics approval

This study was approved by the Medical Ethics Committee of Qingyang Hospital of Traditional Chinese Medicine (Approval No. QYTCM20210011). All procedures involving human participants were performed in accordance with the ethical standards of the 1964 Declaration of Helsinki and its later amendments.

Consent to participate

Written informed consent was obtained from all individual participants included in the study.

Consent for publication

Not applicable.

Competing interest

The authors declare no conflicts of interest and assume sole responsibility for the content and authorship of this manuscript.

Data availability

The data that support the findings of this study are openly available in figshare at http://doi.org/10.6084/m9.figshare.31920846.

Acknowledgements

We extend our gratitude to the Qingyang Hospital of Traditional Chinese Medicine for their invaluable experimental support. Furthermore, the authors affirm that no AI-generated content has been utilized in the preparation of this manuscript.

References

1. Schoettler, M. L. & Nathan, D. G. The Pathophysiology of Acquired Aplastic Anemia: Current Concepts Revisited. *Hematol. Oncol. Clin. North. Am.* **32** (4), 581–594. 10.1016/j.hoc.2018.03.001 (2018).
2. Giudice, V. & Selleri, C. Aplastic anemia: Pathophysiology. *Semin Hematol.* **59** (1), 13–20. 10.1053/j.seminhematol.2021.12.002 (2022).
3. Born, G. et al. Engineering of fully humanized and vascularized 3D bone marrow niches sustaining undifferentiated human cord blood hematopoietic stem and progenitor cells. *J. Tissue Eng.* **12**, 20417314211044855. 10.1177/20417314211044855 (2021).
4. Kandarakov, O., Belyavsky, A. & Semenova, E. Bone Marrow Niches of Hematopoietic Stem and Progenitor Cells. *Int. J. Mol. Sci.* **23** (8), 4462. 10.3390/ijms23084462 (2022).
5. Xu, Y. N. et al. BM-MSCs overexpressing the Numb enhance the therapeutic effect on cholestatic liver fibrosis by inhibiting the ductular reaction. *Stem Cell. Res. Ther.* **14** (1), 45. 10.1186/s13287-023-03276-w (2023).
6. Pan, C. et al. BM-MSCs display altered gene expression profiles in B-cell acute lymphoblastic leukemia niches and exert pro-proliferative effects via overexpression of IFI6. *J. Transl Med.* **21** (1), 593. 10.1186/s12967-023-04464-1 (2023).
7. Yin, X. H. et al. lncRNA HHIP-AS1/HHIP modulates osteogenic differentiation of BM-MSCs by regulating Hedgehog signaling pathway. *Aging (Albany NY)*. **14** (21), 8839–8855. 10.18632/aging.204381 (2022).
8. Tripathi, A. K. et al. Withaferin A Ameliorated the Bone Marrow Fat Content in Obese Male Mice by Favoring Osteogenesis in Bone Marrow Mesenchymal Stem Cells and Preserving the Bone Mineral Density. *ACS Pharmacol. Transl Sci.* **7** (9), 2621–2636. 10.1021/acsptsci.3c00356 (2024).
9. Zhang, X. et al. FZD6 mediates the contributing role of miR-199a-5p in the adipogenesis of bone marrow mesenchymal stem cells derived from aplastic anemia. *Sci. Rep.* **15** (1), 38865.

10.1038/s41598-025-22732-6 (2025).

10. Zhang, X. et al. Chidamide suppresses adipogenic differentiation of bone marrow derived mesenchymal stem cells via increasing REEP2 expression. *iScience* **26** (3), 106221. 10.1016/j.isci.2023.106221 (2023).
11. DeVeaux, S. A. et al. Characterizing human mesenchymal stromal cells' immune-modulatory potency using targeted lipidomic profiling of sphingolipids. *Cytotherapy* **24** (6), 608–618. 10.1016/j.jcyt.2021.12.009 (2022).
12. Zhang, Y. et al. Integrating network pharmacology and experimental validation to explore the mitophagy-associated pharmacological mechanism of modified Shisiwei Jianzhong decoction against aplastic anemia. *Biomed. Chromatogr.* **38** (10), e5963. 10.1002/bmc.5963 (2024).
13. Cai, H., Dong, L. Q. & Liu, F. Recent Advances in Adipose mTOR Signaling and Function: Therapeutic Prospects. *Trends Pharmacol. Sci.* **37** (4), 303–317. 10.1016/j.tips.2015.11.011 (2016).
14. Liu, Z. et al. *Deciphering the physical properties of cell fate decision making in mTOR signaling.* Phys Rev E, 112(2 – 1): p. 024409. (2025). 10.1103/tgzc-vr4q
15. Liu, Y. et al. Author Correction: Ammonia promotes the proliferation of bone marrow-derived mesenchymal stem cells by regulating the Akt/mTOR/S6k pathway. *Bone Res.* **10** (1), 57. 10.1038/s41413-022-00215-y (2022).
16. Chen, G. et al. Structural characterization and anti-inflammatory activity of polysaccharides from Astragalus membranaceus. *Int. J. Biol. Macromol.* **241**, 124386. 10.1016/j.ijbiomac.2023.124386 (2023).
17. Chiu, M. L. et al. Chinese Herbal Medicine Therapy Reduces the Risks of Overall and Anemia-Related Mortalities in Patients With Aplastic Anemia: A Nationwide Retrospective Study in Taiwan. *Front. Pharmacol.* **12**, 730776. 10.3389/fphar.2021.730776 (2021).
18. Chen, Y. et al. Astragalus polysaccharide prevents ferroptosis in a murine model of experimental colitis and human Caco-2 cells via inhibiting NRF2/HO-1 pathway. *Eur. J. Pharmacol.* **911**, 174518. 10.1016/j.ejphar.2021.174518 (2021).
19. Sha, W. et al. Astragalus polysaccharide ameliorates vascular endothelial dysfunction by stimulating macrophage M2 polarization via potentiating Nrf2/HO-1 signaling pathway. *Phytomedicine* **112**, 154667. 10.1016/j.phymed.2023.154667 (2023).
20. Wei, Y. et al. Astragalus polysaccharide attenuates bleomycin-induced pulmonary fibrosis by inhibiting TLR4/ NF-kappaB signaling pathway and regulating gut microbiota. *Eur. J. Pharmacol.* **944**, 175594. 10.1016/j.ejphar.2023.175594 (2023).
21. Kanehisa, M., Furumichi, M., Sato, Y., Matsuura, Y. & Ishiguro–Watanabe, M. KEGG: biological systems databaseas a model of the real world. *Nucleic Acids Res.* **53** (D1), D672–D677. 10.1093/nar/gkae909 (2025).
22. Kanehisa, M. Toward understanding the origin and evolution of cellular organisms. *Protein Sci.* **28** (11), 1947–1951. 10.1002/pro.3715 (2019).

23. Kanehisa, M. & Goto, S. KEGG: kyoto encyclopedia of genes and genomes. *Nucleic Acids Res.* **28** (1), 2730. 10.1093/nar/28.1.27 (2000).
24. Bueno, C. et al. Bone marrow mesenchymal stem cells from patients with aplastic anemia maintain functional and immune properties and do not contribute to the pathogenesis of the disease. *Haematologica* **99** (7), 1168–1175. 10.3324/haematol.2014.103580 (2014).
25. Liu, X. et al. Bone marrow mesenchymal stem cell-derived exosomes attenuate cerebral ischemia-reperfusion injury-induced neuroinflammation and pyroptosis by modulating microglia M1/M2 phenotypes. *Exp. Neurol.* **341**, 113700. 10.1016/j.expneurol.2021.113700 (2021).
26. Wang, X. A. et al. *Mesenchymal Stem Cells in Acquired Aplastic Anemia: The Spectrum from Basic to Clinical Utility*. *Int. J. Mol. Sci.* **24**(5):4464. 10.3390/ijms24054464

Figures

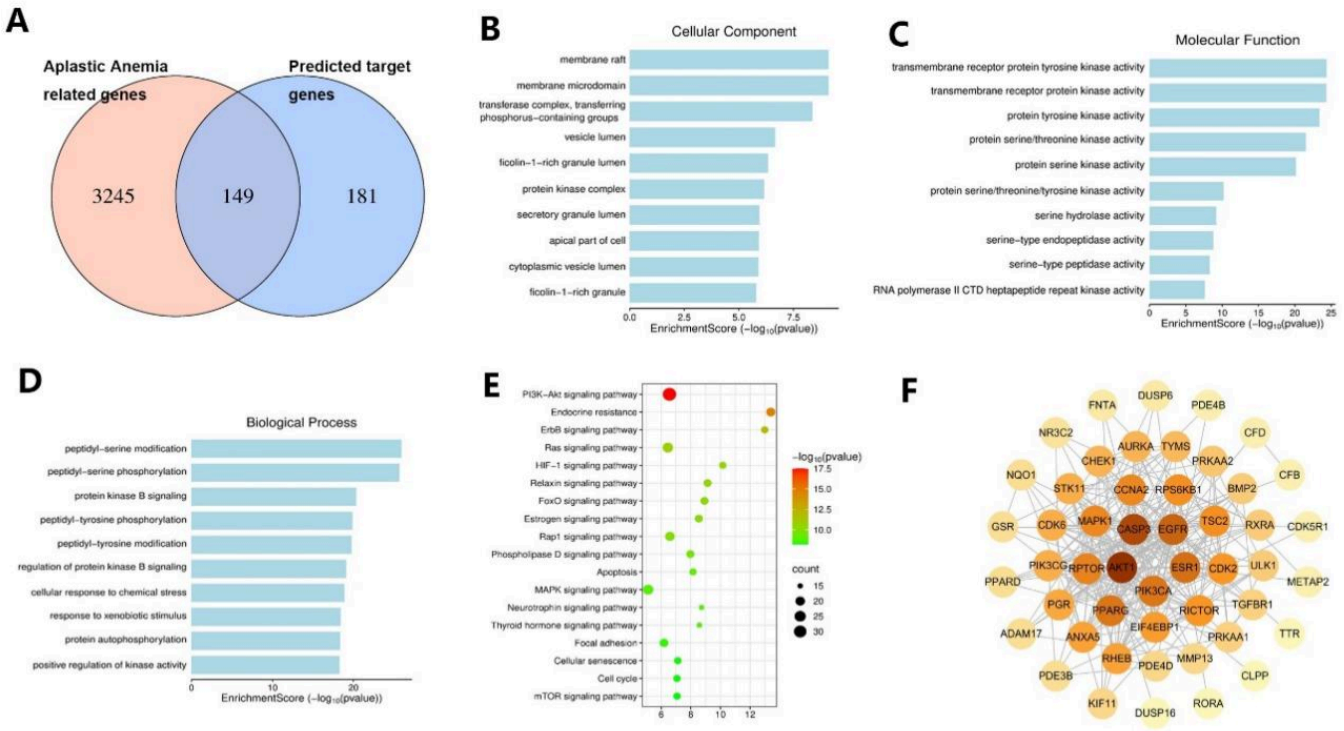


Figure 1

Integrated network pharmacology analysis of Astragalus membranaceus in aplastic anemia. (A) Venn diagram showing the overlap between AA-related genes and predicted targets of Astragalus. (B) Cellular component, (C) molecular function, and (D) biological process enrichment of shared targets. (E) KEGG pathway enrichment; dot size indicates gene count, color represents -$\log_{10}$(p-value).KEGG pathway enrichment analysis was conducted relying on annotated datasets retrieved from the KEGG database (https://www.genome.jp/kegg/). All copyrighted KEGG pathway maps presented in the figure have

obtained formal copyright permission from Kanehisa Laboratories.[21-23]. (F) Protein-protein interaction (PPI) network of core targets; hub genes are highlighted.

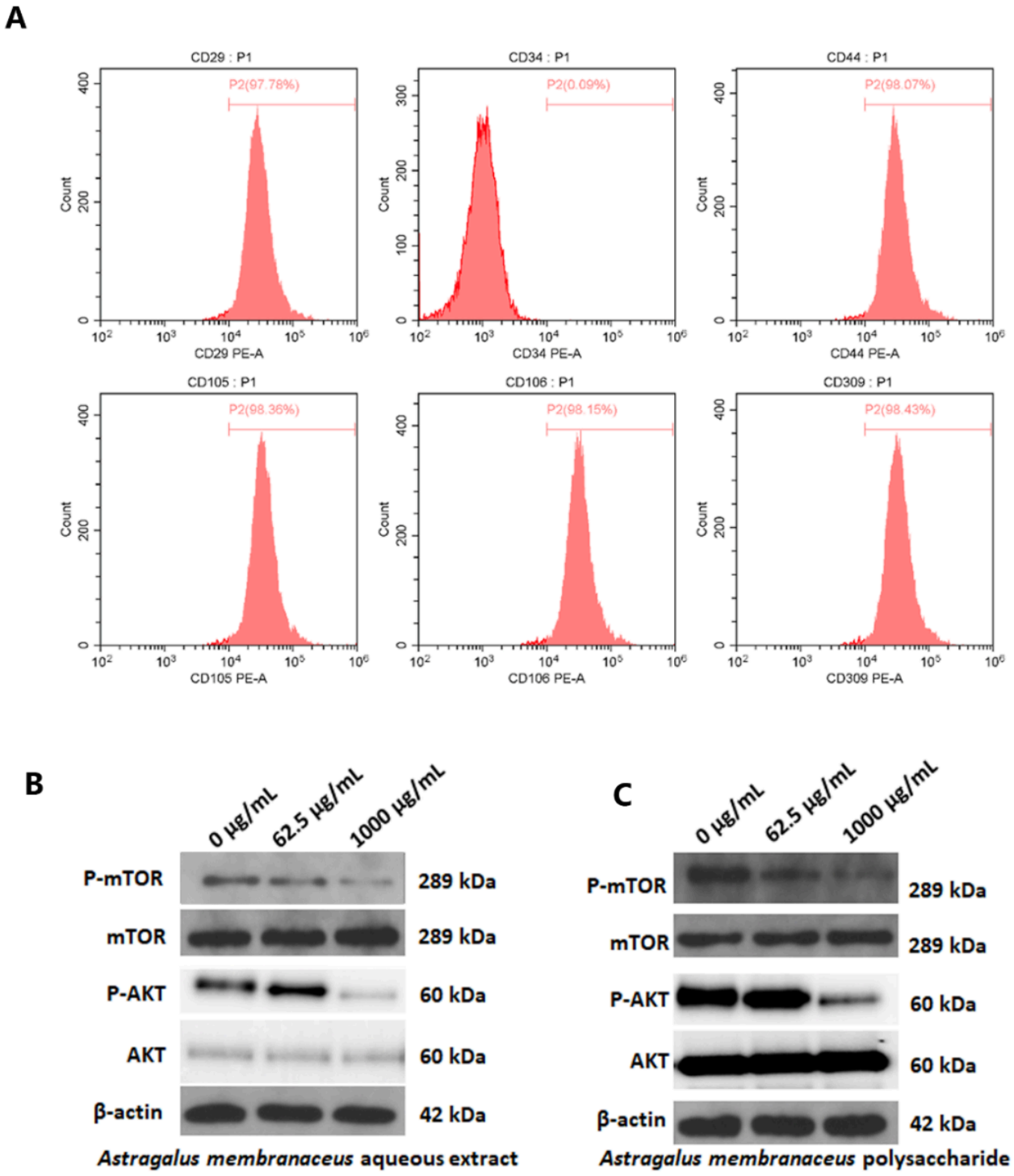


Figure 2

Phenotypic validation of AA-BM-MSCs and dose-dependent effects of Astragalus preparations on PI3K-AKT-mTOR signaling. (A) Flow cytometric profiles showing characteristic MSC marker expression. (B)

Western blot analysis of p-AKT, AKT, p-mTOR, mTOR, and β-actin in AA-BM-MSCs treated for 48 h with APS (62.5 and 1000 μg/mL). (C) Western blot analysis of p-AKT, AKT, p-mTOR, mTOR, and β-actin in AA-BM-MSCs treated for 48 h with AQE (62.5 and 1000 μg/mL, expressed as crude herb equivalent).

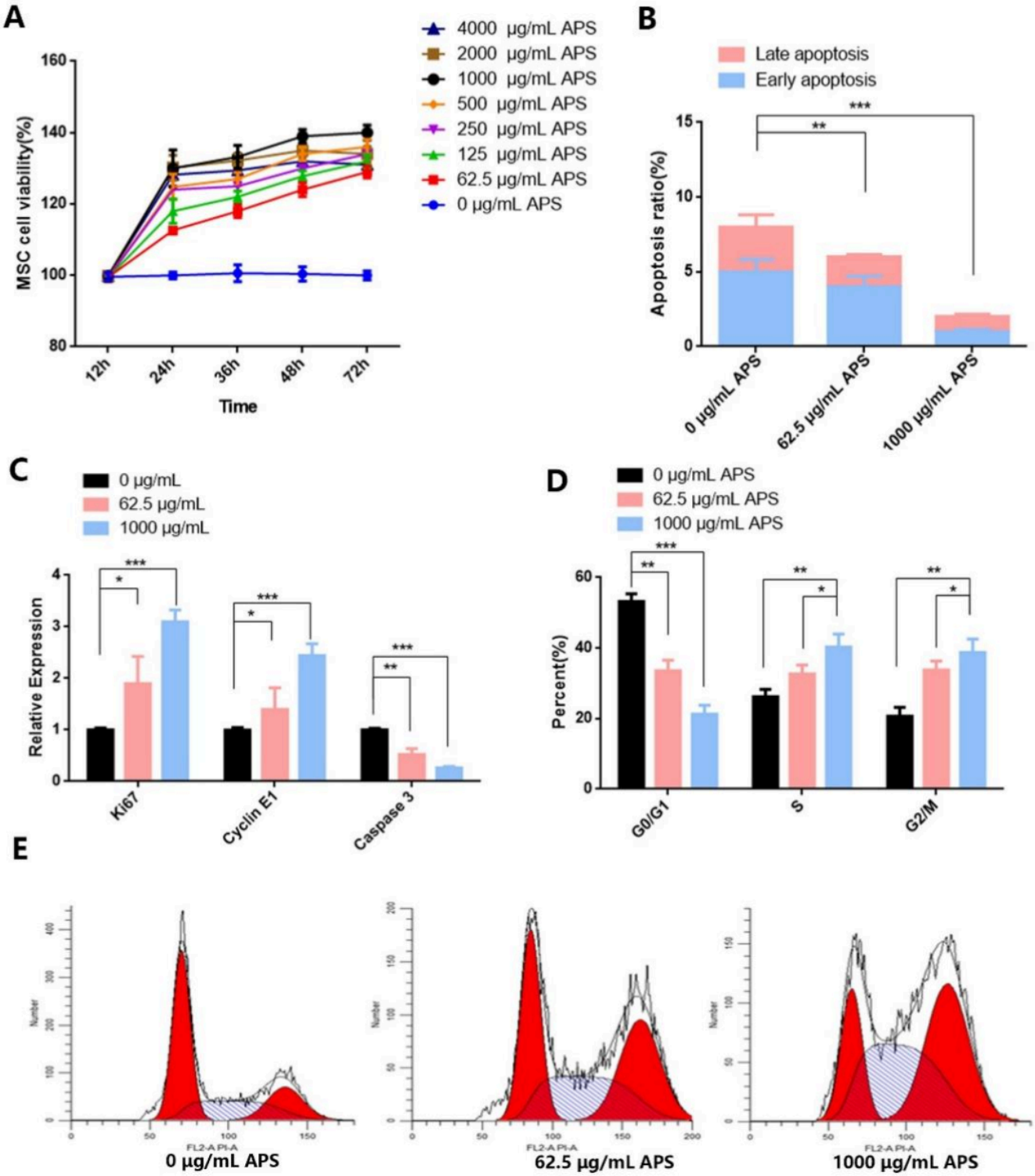


Figure 3

Effects of APS at different mass concentrations on the proliferation of BM-MSCs from patients with AA. (A) CCK-8 assay showing time and concentration-dependent effects of APS on cell viability. (B) Representative flow cytometry dot plots of Annexin V-FITC/PI staining. (C) Quantification of total apoptotic cells. (D) Cell cycle distribution quantification. (E) Representative histograms of PI staining for cell cycle analysis.

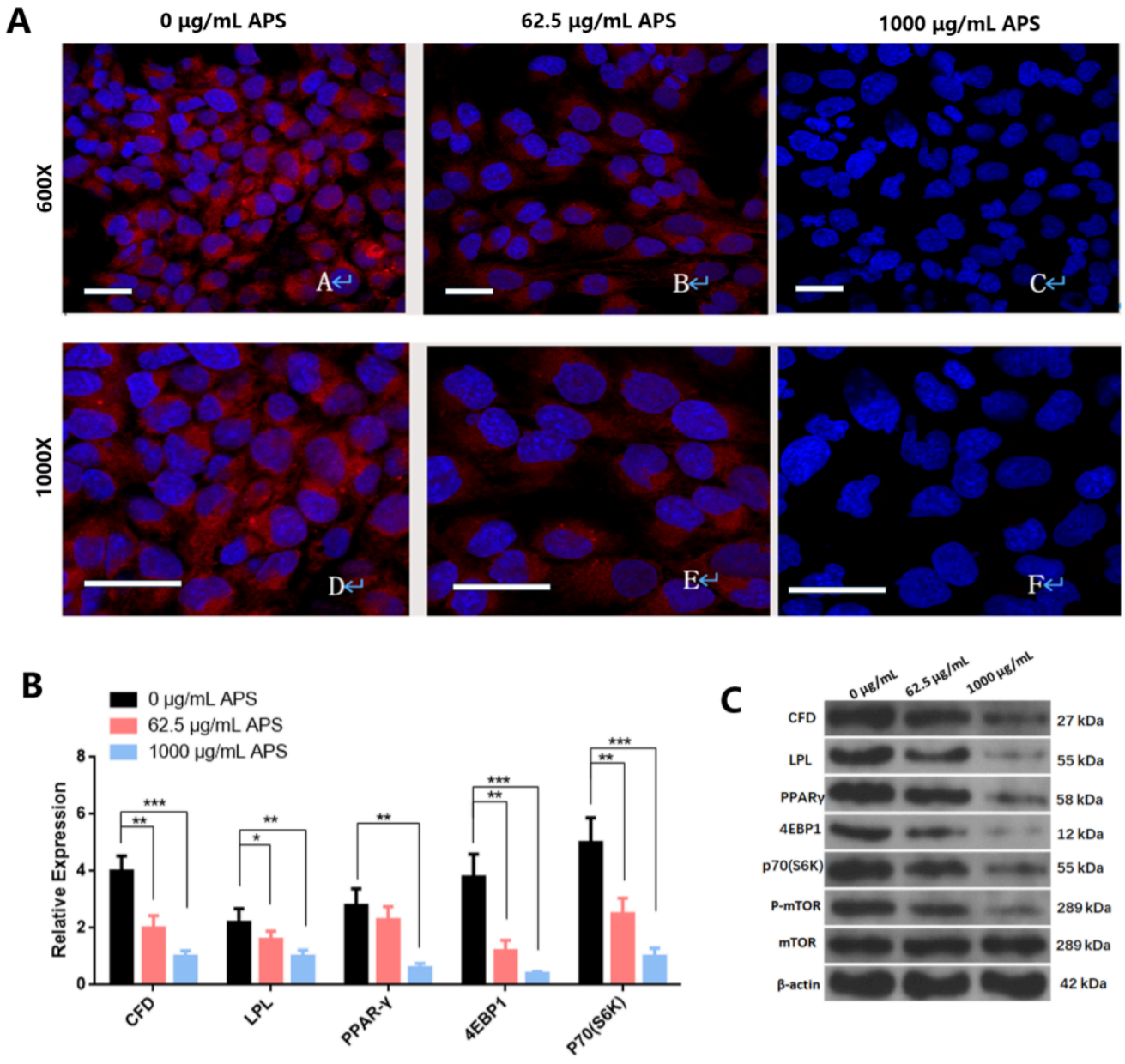


Figure 4

Molecular mechanisms of APS-mediated suppression of adipogenesis in AA-BM-MSCs. (A) Representative confocal images of lipid accumulation stained with Nile red (scale bar = 20 μm). (B) qRT-PCR analysis of CFD, LPL, PPARγ, 4EBP1, and P70S6K mRNA expression. (C) Western blot analysis of CFD, LPL, PPARγ, 4E-BP1, p70S6K, mTOR, and p-mTOR protein levels; β-actin served as loading control.

Supplementary Files

This is a list of supplementary files associated with this preprint. Click to download.

- SupplementaryTableS1.SequencesofRealtimePCRprimers.xlsx
- SupplementaryTableS2.BioactivecompoundsofAstragalusm.xlsx
- Supplementaryfigures.docx